Incoherent Branched Flow of Light

Anatoly Patsyk,[1,3] Yonatan Sharabi,[1,3] Uri Sivan,[1,3] and Mordechai Segev[1,2,3]

[1]*Physics Department, Technion-Israel Institute of Technology, Haifa 3200003, Israel*
[2]*Electrical Engineering Department, Technion-Israel Institute of Technology, Haifa 3200003, Israel*
[3]*Solid State Institute and the Russell Berrie Nanotechnology Institute, Technion, Haifa 3200003, Israel*

(Received 15 November 2021; accepted 9 February 2022; published 11 April 2022)

Waves traveling in weakly disordered media possessing long-range correlations experience a universal phenomenon known as branched flow, where the waves split and form channels (branches) of enhanced intensity that keep dividing as the waves propagate. Branched flow effects have been studied experimentally in various systems, thus far always with coherent waves. We present the first experimental observation of branched flow of spatially incoherent light. We show that the primary effect of branching occurs for both coherent and incoherent light, but each pronounced branch is accompanied by sidelobes arising from interference, which disappear when the waves are incoherent. The position of the first caustic, where the branches reach peak intensity, remains the same as the coherence is reduced, but the branch statistics changes and some branches blur or disappear.

DOI: 10.1103/PhysRevX.12.021007 Subject Areas: Optics, Photonics

Waves scattered from weak disorder with spatial correlation distance longer than the wavelength tend to form long collimated branches. This propagation regime is intermediate between random speckle patterns (characterizing scattering in random potential) and regular beam diffraction-broadening akin to homogeneous media such as free space. In this intermediate regime, multiple high-intensity caustics emerge, and the propagation of waves is reminiscent of lightning branches or river deltas. This phenomenon, known as branched flow (BF), was first observed for electrons in a 2D electron gas [1–8], microwave in resonators [9,10], and, very recently, with laser light propagating in thin soap membranes [11]. However, BF is a ubiquitous phenomenon expected with other waves such as sound waves [12], relativistic particles [13], and more [14]. Moreover, despite its linear nature, BF can also occur under nonlinear conditions, where it may trigger nonlinear waves [15–17] or extreme ("rogue") waves [18–21]. On larger scales, BF has also been suggested to explain focusing of tsunami waves [22–24] or rare freak waves in the middle of the ocean. Over the years, various properties of BF have been studied theoretically, including the number of branches [25], the statistical distribution of their peaks [26,27], energy stability [28], BF in anisotropic potentials [29], and BF shaping [30]. In these studies, BF is mostly treated in the framework of ray optics caustics, neglecting coherence or interference effects [14,31]. Experiments, on the other hand, were thus far carried out only with coherent waves, such as coherent electron waves [1], coherent microwave [9,10], or with coherent laser light [30]. This gap between experiments and theory naturally raises fundamental questions regarding the role of coherence in the formation and evolution of BF. Does BF result from coherent interference between the different wave fronts and is therefore sensitive to the wavelength and to the coherence of the waves, or is it dictated by ray scattering off correlated disorder, which was the original explanation for the observation of BF [1]? Furthermore, if BF also appears in the incoherent regime, does interference change its statistical properties such as scintillation index and wave statistics? Thus far, all experiments use coherent wave sources, while BF with incoherent waves is considered only in simulations [32,33]. The question of whether and how interference plays a role in BF is, therefore, open.

Here, we present the first experimental study of the effect of spatial coherence on BF of light. We couple an optical beam of controllable coherence into a thin liquid soap film and study the evolution and statistics of BF within this film. The light propagating within the soap film experiences scattering from thickness variations that act as a two-dimensional medium with a random (yet correlated) variation in the index of refraction. We find that BF with incoherent light is qualitatively different than with coherent light. The former shows fewer branches, and their intensity distribution is narrower, implying that very high and very low intensity peaks are rare. Our study elucidates the effect of coherence and interference on BF, allowing for the design of future experiments with partially coherent waves.

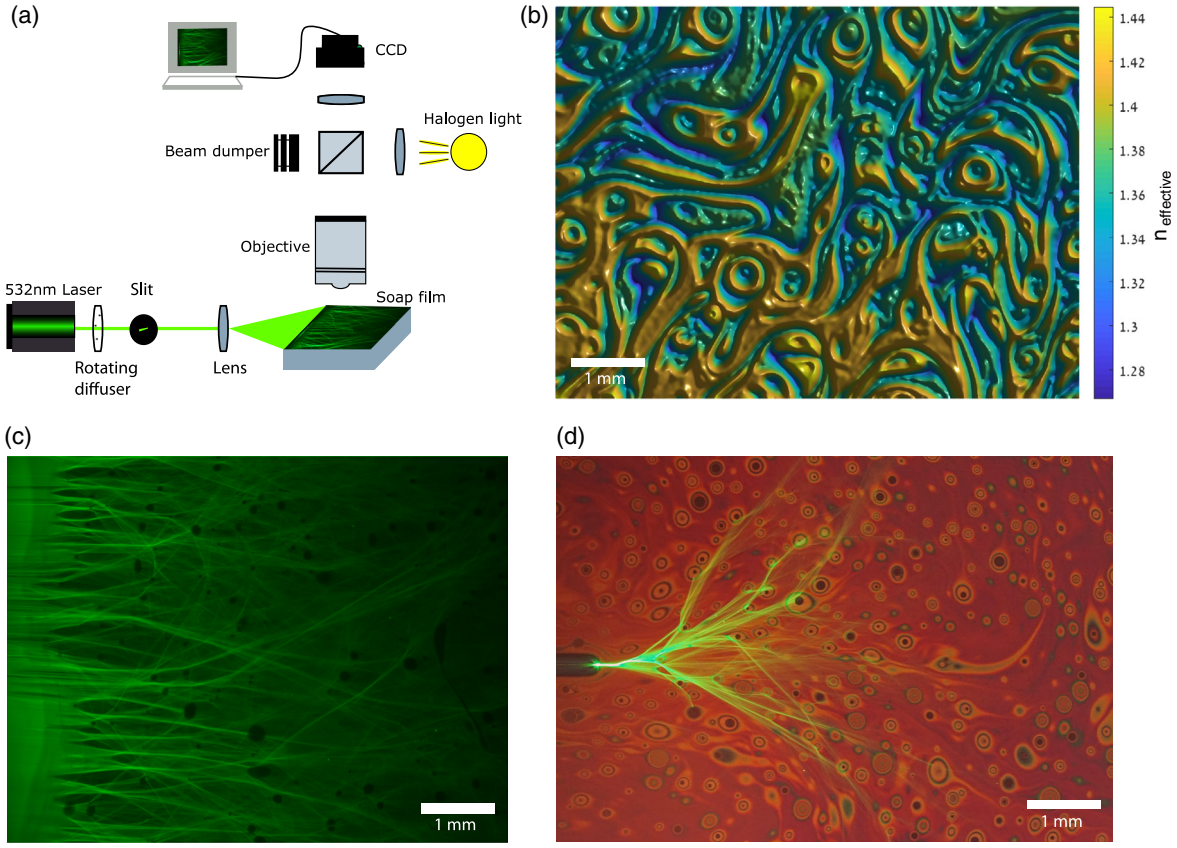

FIG. 1. (a) Experimental setup showing the main components, the path the light beam follows, and the imaging system. (b) Effective refractive index landscape of a soap film reconstructed using DNN from an image of the halogen light reflected from the film. (c) BF generated by a coherent plane wave. (d) BF generated by a localized source coupled to the film (the fiber tip seen on the left).

In our experiment, we generate a partially spatially incoherent quasimonochromatic wave by passing a laser beam through a diffuser and then coupling it into a thin soap film, as previously reported with coherent light [11]. It is important to note that BF does not occur naturally in soap films for arbitrary conditions. Rather, the conditions must be adjusted to enable thickness variations in the proper range of parameters; otherwise, the emerging patterns would be waveguiding channels where the effective refractive index is higher, or a nonlinear process such as surface polariton formation [34], or guiding by deformation of the membrane by optical forces [35], or no patterns at all.

To compare BF under different coherence conditions, we use three different sources: as a coherent plane wave (as in Ref. [11]), a speckled coherent wave (obtained by passing the laser beam through a diffuser), and a partially-spatially-incoherent wave formed by rotating the diffuser. All three waves use the same 532 [nm] cw laser source. After the diffuser, the beam is passed through a narrow slit to truncate sidelobes and facilitate efficient light coupling into the film. The slit is then imaged on the entrance plane of the film. The experimental system is displayed in Fig. 1(a). When the laser beam passes through the diffuser, it acquires a spatially random phase and amplitude speckled pattern with a Gaussian envelope in momentum space (k space) [36]. When the diffuser is rotating, the beam partially loses its spatial coherence. The spatial correlation distance corresponds to the mean speckle size that can be estimated by stopping the diffuser rotation and imaging the speckled pattern onto a camera.

Our experimental setup allows for simultaneous mapping of the membrane thickness, which, in turn, dictates the local effective index of refraction. To that end, we shine white light from a halogen lamp perpendicular to the film and measure the reflection. The thin film acts as a Fabry-Perot resonator with a frequency-dependent reflection coefficient, depending on the local thickness of the film. The resulting color map is translated, using a deep neural network (DNN) algorithm, to a thickness map and the effective refractive index landscape shown in Fig. 1(b). As shown in Supplemental Material [37], the DNN-based method provides superior reconstruction compared with the method used in Ref. [11].

The propagation of light and its branching are observed by imaging the light emitted from fluorescent rhodamine molecules embedded in the film. The fluorescence intensity pattern is imaged onto a camera positioned above the film. A band-stop spectral filter centered around 532 nm is used

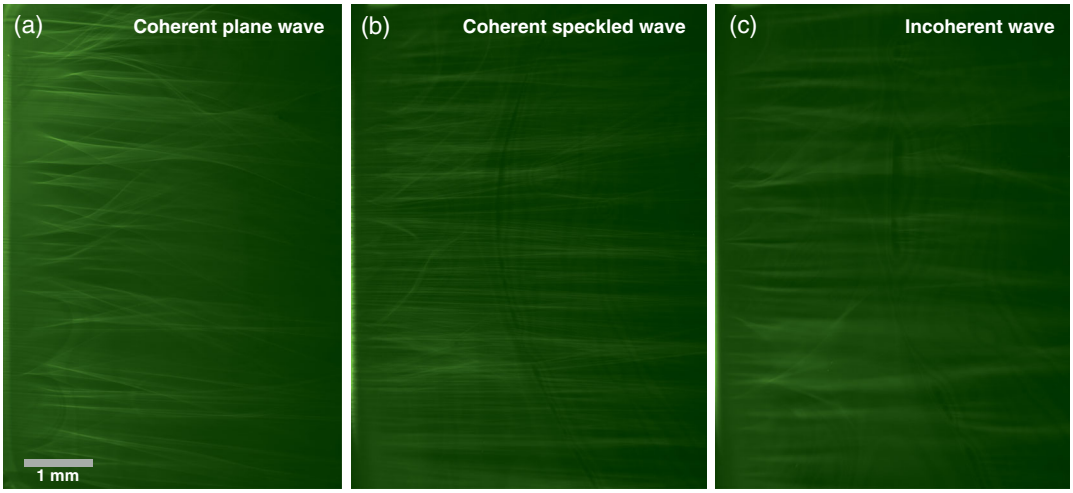

FIG. 2. Examples of branched flow patterns formed by (a) coherent plane wave, (b) coherent speckled beam generated by passing a coherent plane wave through a static diffuser, (c) partially-spatially-incoherent beam, generated by passing a coherent plane wave through the same diffuser while rotating.

to separate the longer-wavelength light emitted from the rhodamine molecules from the residual light coming from other sources. The camera records movies of the fluorescent light patterns as they evolve in time. Snapshots of the images are shown in Figs. 1(c) and 1(d), displaying BF patterns generated by a coherent plane wave input (c) and a coherent localized input injected from a fiber tip (acting as a highly localized source) (d). The branches and finer features associated with BF can be seen in both images.

The degree of spatial coherence can be estimated by measuring the mean speckle size upon the beam. Alternatively, the correlation distance of the diffused light can be calculated from the diffraction angle of the partially-spatially-incoherent beam in free space. In the limit of quasihomogeneous partially-spatially-incoherent light [38,39], the diffraction angle (under the paraxial approximation) equals the ratio between the wavelength and the correlation distance.

When a beam passes through a rotating diffuser, the spatially random speckle pattern changes in time and, when imaged by a slow camera (or the human eye), yields an ensemble average over realizations of speckle patterns of the same statistical features. The BF observed with incoherent light corresponds to averaging over numerous different speckled patterns launched into the film, each showing its own branching pattern as it scatters from the exact same thickness variations. Thus, branched flow of partially incoherent waves is essentially an ensemble average over multiple realizations of speckled beams with the same correlation properties, each forming its own BF pattern. For these reasons, we compare the incoherent BF to the BF generated by two different coherent sources: a pristine plane wave and a beam passing through the same diffuser when static [Figs. 2(a)–2(c)]. The spatially incoherent beam generated by the rotating diffuser and the speckled beam generated by the same diffuser when it is static share the same (ensemble-averaged) spectral distribution in k space.

Comparing the BF patterns formed by coherent and incoherent light beams, we find qualitative differences (Fig. 2). Most fine features and some branches observed with spatially coherent light are missing with spatially incoherent light. The small sidelobes accompanying pronounced branches wash out while leaving the more pronounced branches intact. Furthermore, the peak intensity of the pronounced branches is higher with coherent light. This observation is highlighted by Fig. 3 that shows BF patterns formed by coherent (a) and incoherent (b) beams traveling in the same refractive index landscape. The corresponding intensity of the image along the cuts marked by the full and dashed red lines in Fig. 3(a) are depicted in Figs. 3(c) and 3(d) for the coherent (blue lines) and incoherent waves (red lines). The BF pattern generated by the coherent wave shows many more channels, and sharper peaks of variable heights. Figure 3(e) enlarges the region marked in Fig. 3(c), highlighting differences in the intensity landscape surrounding the main branches. As seen, the pronounced intensity peaks associated with the main branches occur largely at the same positions, but their visibility is lower in the incoherent case, and—more importantly—the sidelobes that accompany the main branches in the coherent case do not show in the incoherent case. This observation implies the existence of two different mechanisms involved in the formation of BF: one common to coherent and incoherent light and the other showing only with coherent light. The first mechanism is traced to ray optics caustics, while the second mechanism to the presence of interference effects between partial waves corresponding to the caustics. Namely, the main channels are a direct result of the formation of caustics via scattering from the potential landscape, expressed by the local variations in

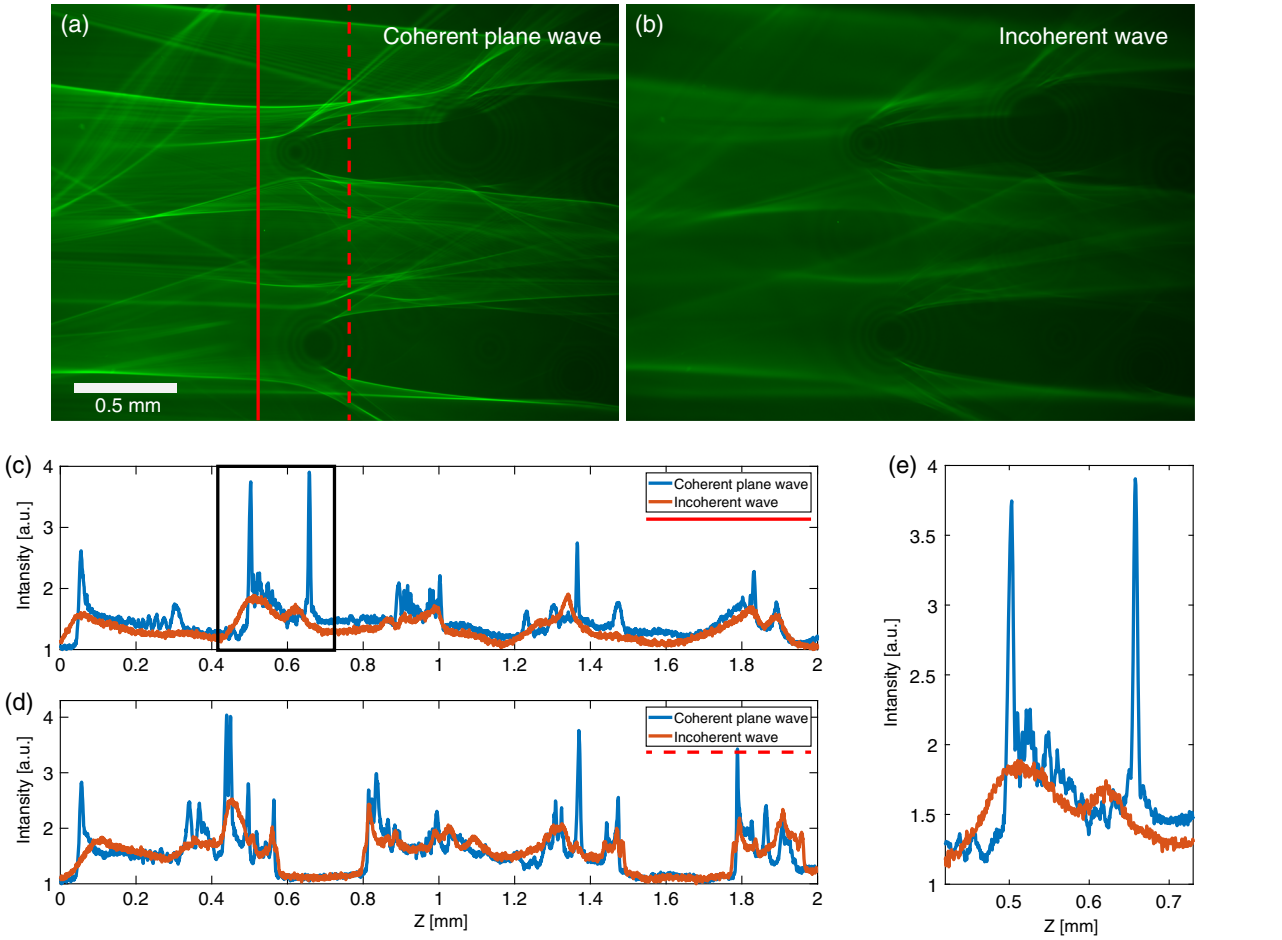

FIG. 3. (a),(b) BF intensity patterns observed in the same region of the soap film for a coherent plane wave (a) and an incoherent wave (b). The two images demonstrate the smearing effect of incoherence smoothening the intensity pattern and concealing the coherent features. (c),(d) Intensity cross section taken along the full (c) and dashed (d) red lines in (a) and (b) (blue and red plots, respectively). The cross sections highlight the stark contrast between the two BF patterns. (e) Enlargement of the region marked in (c), highlighting the difference in the region surrounding each BF channel.

the effective refractive index map. They do not require coherence to form and can be explained by ray optics density calculations—using geometrical optics. From the geometrical optics viewpoint, these channels are caustics, each created by passing rays through a focusing or defocusing region of the potential. A caustic describes the envelope of a family of parallel rays [40]. A caustic does not rely on interference effects; hence, the caustics in our experiments do not disappear when the light loses coherence [33]. On the other hand, the other type of features appearing in the BF patterns arise from interference between the scattered waves: both between waves scattered from the same local region and between waves scattered from different regions in potential landscape. This is a coherent effect that relies on waves having well-defined phases for times longer than the integration time of the camera. When the diffuser rotates fast enough, the relative phases vary in time, the interference effects are lost, and the intensity reduces to a sum of local intensities of the wave.

To explain the experimental observations, we resort to the theory of partially-spatially-incoherent waves and study BF in this framework. The rotating diffuser generates random waves with the same statistics (same speckle size). These waves serve as the initial conditions for the light launched into the thin film and forming the branched flow phenomenon. Each of the random input waves evolves in the two-dimensional soap film into a different realization of the BF pattern. To simulate the evolution, we solve the paraxial wave equation with a fixed 2D refractive index distribution and different initial random field amplitudes of the same statistics. We calculate the emerging random BF patterns and sum their intensities to obtain the intensity distribution captured by the camera in the experiments. In the paraxial approximation, the spatial component of the electric field for a given realization of the specked field can be written as

$$E_i(x,z) = \mathrm{Re}\{U_i(x,z)]e^{-ikz}\}. \quad (1)$$

Here, x and z correspond to the transverse and longitudinal propagation directions, respectively, k is the mean longitudinal wave number, and $U_i(x,z)$ is the 2D spatial distribution of the field in the ith realization, determined by the refractive index landscape and the initial condition $U_i(x,z=0)$ (for a detailed derivation, see Supplemental Material of Ref. [11]). The time-averaged intensity is given (in proper units) by

$$I(x,z)=\sum_i |U_i(x,z)|^2. \tag{2}$$

When the diffuser is stationary, the intensity is described by a single field realization $I_i(x,z)=|U_i(x,z)|^2$. When the diffuser rotates, the intensity is the sum of the intensities of all the different BF realizations generated by the same refractive index landscape (the film is stable enough to guarantee numerous realizations of initial conditions at a fixed potential landscape). The BF pattern evolves instantaneously (scattering occurs at the speed of light in the medium), while the initial conditions vary as the diffuser rotates. In our simulations, we use the refractive index distribution obtained directly from the reflection of the halogen light in our experimental system; hence, the simulation preserves the unique long-range correlations that lead to BF. The simulation consists of the evolution of a set of equations for $U_i(x,z)$, according to Ref. [11]:

$$i\frac{\partial U_i}{\partial z}=\frac{\nabla_\perp^2 U_i}{2kn}+\frac{k_0}{2n}(n_{\mathrm{eff}}^2(r)-n^2)U_i, \tag{3}$$

where n is the background refractive index of the film, k_0 is the wave number in free space, and $n_{\mathrm{eff}}(r)$ is the spatially dependent effective refractive index of the film measured

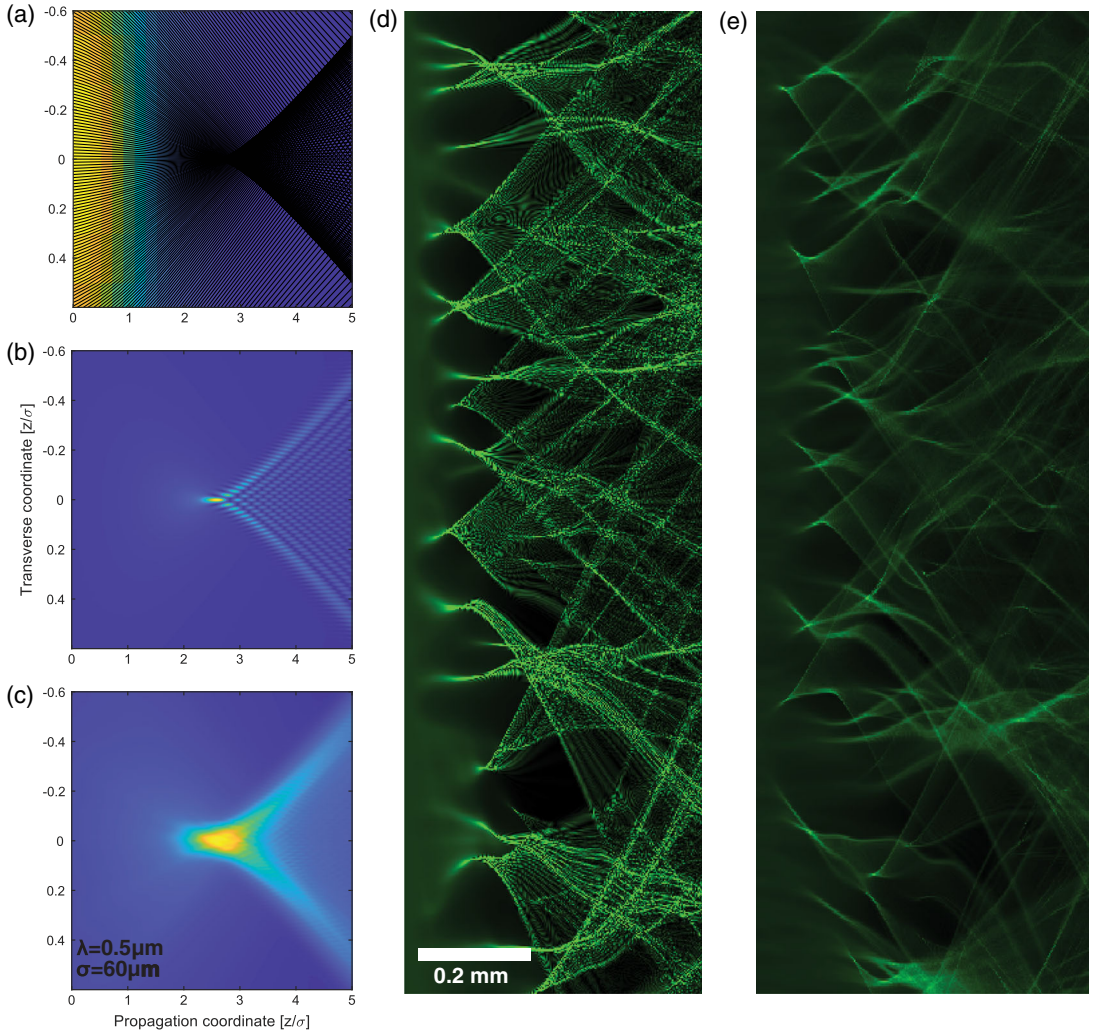

FIG, 4. (a)–(c) Intensity patterns produced by a single scatterer in (a) ray optics simulation and (b),(c) wave propagation simulations of an incident coherent and partially-spatially-incoherent beam in the paraxial approximation, respectively. (a) shows the ray structure of the scattered light forming caustics. (b) shows the main caustic lobes accompanied by weaker sidelobes and interference pattern. (c) shows two branches with no sidelobes and interference pattern. The main lobes are common to all three cases. (d),(e) Simulation of coherent and incoherent BF in a specific realization of refractive index landscape reconstructed from the experiment.

by reflection of halogen light from the 2D film as detailed in Ref. [11]. To simulate the input of a coherent plane wave, we simply use uniform amplitude and phase at the input. For the wave passing through the static diffuser, we use the speckle size imaged in the experiment to form a spatially random field distribution that serves as the input speckled field. Finally, to simulate the incoherent wave, we generate an ensemble of 1000 realizations of the coherent speckled wave and sum the intensities of the emerging BF patterns.

To illustrate the difference between the three cases, we start with the simple case of waves scattering off a single Gaussian scatterers of diameter 60 μm (Fig. 4) calculated in the ray optics approximation (a), coherent speckled wave (b), and spatially incoherent wave (c). Ray caustics are evident in all three cases. As expected, Fig. 4(a) lacks any sidelobes or finer features. Figure 4(b) displays two main bright lobes following the caustics of Fig. 4(a), as well as a rich pattern of sidelobes arising from interference. Figure 4(c) displays the simulated evolution of the partially-spatially-incoherent beam scattering off a single scatterer. The figure shows that the interference pattern is smeared out upon averaging over 1000 initial coherent speckled beams, leaving behind the two main caustic lobes. The same effect of incoherence is evident for the experiments of light propagation in the soap film where multiple scattering occurs. Branched flow is clearly observed with both coherent [Fig. 4(d)] and incoherent light [Fig. 4(e)], but the fine features observed with coherent light are averaged out when incoherent light is used. The same qualitative effect of incoherence can be seen by comparing Fig. 2(a) to Fig. 2(c) or Fig. 3(a) to Fig. 3(b). These results indicate that coherence is not a prerequisite for the

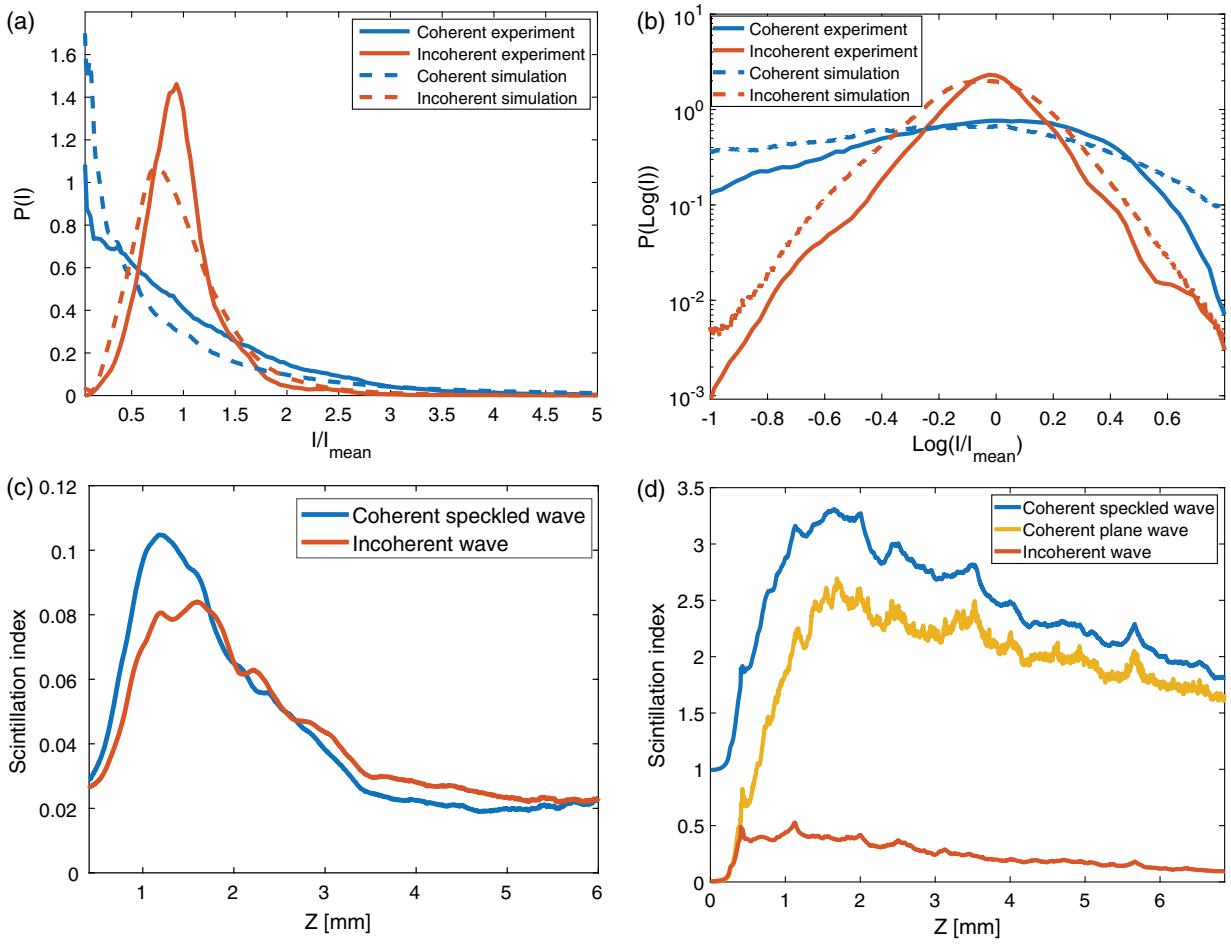

FIG. 5. (a) Probability distribution of coherent and incoherent BF intensity as observed in experiments and in simulations. The intensity distribution of BF is narrower for spatially incoherent light, and the probability to observe very high or low intensities is smaller than for the coherent waves. (b) The same data as in (a) on a $P[\mathrm{Log}(I)] - \mathrm{Log}(I/I_{\mathrm{mean}})$ scale. The coherent distribution is broad, while the incoherent one is concentrated around the mean. (c) Scintillation index along the propagation direction calculated from experimental data. The similar peak position discloses that branching starts at the same distance for coherent and spatially incoherent light. The measured values in (c) are reduced (compared to the true values) by additional background light, which is inevitable when coupling a multimode (or incoherent) beam into a thin film. (d) Scintillation index calculated from simulations for coherent, speckled, and incoherent waves. Branching starts at the same distance for all cases, but the intensity fluctuations are markedly different.

formation of BF, but the fine details—apparent in experiments and simulations—are governed by interference effects which are affected by coherence. Interference also affects the peak intensities of the branches, which are much higher in the coherent case.

Having reviewed the qualitative differences between coherent and incoherent BF, we turn to analyze the effect of incoherence on the statistical properties of BF, namely, intensity distribution and scintillation index. For the simulations, we use nine reconstructed membranes; for the incoherent beam, we average over 1000 realizations of BF for each membrane. The comparison between experiments and theory helps to pinpoint the differences between the statistical signature of coherent and incoherent BF. The main advantage of simulations is the large signal-to-noise (SNR) ratio, enabling detection of low-intensity features that are masked in our experimental system due to background noise.

Figures 5(a) and 5(b) display the experimental and simulated intensity distribution of BF plotted on a linear (a) and a log-log (b) scale, normalized such that $I = 1$ is the value of the mean light intensity in the film. These distributions are taken at the propagation distance corresponding to the peak of the scintillation index, where the fluctuations are the highest. The plots reveal a stark difference between coherent and incoherent BF. The intensity distribution for coherent BF decays as the intensity grows, which is typical for BF statistics [11,20,31,32]. The intensity distribution for incoherent BF, on the other hand, resembles a log-normal distribution with a pronounced peak at the mean intensity, $I = 1$. The distribution is qualitatively different for coherent and incoherent BF, and the probability of having high- and low-intensity peaks is considerably lower for the incoherent case. Namely, there are fewer high-intensity branches and higher background with incoherent light. Note the similarity between the experimental and theoretical results.

Figures 5(c) and 5(d) display the scintillation index of the BF as a function of the propagation distance along the z axis for experimental (c) and simulation (d) data. The scintillation index $S(Z) = \{[I^2(z)]/I(z)^2\} - 1$, calculated by averaging along the transverse dimension, describes the normalized variance of the intensity distribution so that the mean intensity does not affect the result. The maximum of the scintillation index identifies the formation of the first main caustics—the propagation distance at which pronounced branching takes place. As seen in Fig. 5(c), the scintillation index is similar for coherent and incoherent light with the first caustics remaining roughly at the same distance. Simulations [Fig. 5(d)] reveal that the maximal scintillation index appears at similar propagation distances for coherent and incoherent BF. The simulations in Fig. 5(d) show that coherent beams usually produce higher-intensity peaks than the incoherent beams and larger intensity variations, which are even more pronounced for the speckled coherent beam than for the plane wave input. The intensity fluctuations in the incoherent regime are smaller due to the loss of interference effects.

In conclusion, we investigate BF of partially-spatially-incoherent waves and underpin the role of spatial coherence in the BF phenomenon. While the gross features follow ray caustics and do not require coherence, having coherence introduces interference effects manifested in clear sidelobes accompanying each branch. The intensity and log-intensity distribution statistics show that incoherent BF is concentrated around its mean value with a lower probability (compared with coherent light) of high-intensity peaks. Branching (indicated by the peak of the scintillation index) starts at the same distance from the input plane for coherent and incoherent light, granting the scintillation index a universality, which depends solely on the potential landscape (effective refractive index distribution in our specific experiments). Naturally, the scintillation index for incoherent light has smaller intensity fluctuations. All these findings are supported by simulations performed on the experimental refractive index landscape mapped independently with the actual films used in experiments. Incoherent BF is especially important, as most wave sources in nature are at least partially incoherent, such as sunlight or a light bulb. Understanding the behavior of incoherent waves in the context of BF is fundamentally important and highly interesting. It can also shed light on extreme wave phenomena in nature, especially in cases where the high-intensity branches trigger nonlinear phenomena. It should, therefore, be interesting to study BF in the context of incoherent nonlinear waves in highly nonlinear media, as some theoretical studies have recently begun exploring [15].

[1] M. A. Topinka, B. J. LeRoy, R. M. Westervelt, S. E. J. Shaw, R. Fleischmann, E. J. Heller, K. D. Maranowski, and A. C. Gossard, *Coherent Branched Flow in a Two-Dimensional Electron Gas*, Nature (London) **410**, 183 (2001).

[2] K. E. Aidala, R. E. Parrott, T. Kramer, E. J. Heller, R. M. Westervelt, M. P. Hanson, and A. C. Gossard, *Imaging Magnetic Focusing of Coherent Electron Waves*, Nat. Phys. **3**, 464 (2007).

[3] M. P. Jura, M. A. Topinka, L. Urban, A. Yazdani, H. Shtrikman, L. N. Pfeiffer, K. W. West, and D. Goldhaber-Gordon, *Unexpected Features of Branched Flow through High-Mobility Two-Dimensional Electron Gases*, Nat. Phys. **3**, 841 (2007).

[4] D. Maryenko, F. Ospald, K. v. Klitzing, J. H. Smet, J. J. Metzger, R. Fleischmann, T. Geisel, and V. Umansky, *How Branching Can Change the Conductance of Ballistic Semiconductor Devices*, Phys. Rev. B **85**, 195329 (2012).

[5] B. Liu and E. J. Heller, *Stability of Branched Flow from a Quantum Point Contact*, Phys. Rev. Lett. **111**, 236804 (2013).

[6] A. A. Kozikov, C. Rössler, T. Ihn, K. Ensslin, C. Reichl, and W. Wegscheider, *Interference of Electrons in Backscattering through a Quantum Point Contact*, New J. Phys. **15**, 013056 (2013).
[7] B. A. Braem, C. Gold, S. Hennel, M. Röösli, M. Berl, W. Dietsche, W. Wegscheider, K. Ensslin, and T. Ihn, *Stable Branched Electron Flow*, New J. Phys. **20**, 073015 (2018).
[8] K. R. Fratus, C. Le Calonnec, R. Jalabert, G. Weick, and D. Weinmann, *Signatures of Folded Branches in the Scanning Gate Microscopy of Ballistic Electronic Cavities*, SciPost Phys. **10**, 069 (2021).
[9] R. Höhmann, U. Kuhl, H.-J. Stöckmann, L. Kaplan, and E. J. Heller, *Freak Waves in the Linear Regime: A Microwave Study*, Phys. Rev. Lett. **104**, 093901 (2010).
[10] S. Barkhofen, J. J. Metzger, R. Fleischmann, U. Kuhl, and H.-J. Stöckmann, *Experimental Observation of a Fundamental Length Scale of Waves in Random Media*, Phys. Rev. Lett. **111**, 183902 (2013).
[11] A. Patsyk, U. Sivan, M. Segev, and M. A. Bandres, *Observation of Branched Flow of Light*, Nature (London) **583**, 60 (2020).
[12] M. A. Wolfson and S. Tomsovic, *On the Stability of Long-Range Sound Propagation through a Structured Ocean*, J. Acoust. Soc. Am. **109**, 2693 (2001).
[13] M. Mattheakis, G. P. Tsironis, and E. Kaxiras, *Emergence and Dynamical Properties of Stochastic Branching in the Electronic Flows of Disordered Dirac Solids*, Europhys. Lett. **122**, 27003 (2018).
[14] E. J. Heller, R. Fleischmann, and T. Kramer, *Branched Flow*, Phys. Today **74**, No. 12, 44 (2021).
[15] G. Green and R. Fleischmann, *Branched Flow and Caustics in Nonlinear Waves*, New J. Phys. **21**, 083020 (2019).
[16] J. M. Dudley, F. Dias, M. Erkintalo, and G. Genty, *Instabilities, Breathers and Rogue Waves in Optics*, Nat. Photonics **8**, 755 (2014).
[17] A. Safari, R. Fickler, M. J. Padgett, and R. W. Boyd, *Generation of Caustics and Rogue Waves from Nonlinear Instability*, Phys. Rev. Lett. **119**, 203901 (2017).
[18] M. Mattheakis, I. J. Pitsios, G. P. Tsironis, and S. Tzortzakis, *Extreme Events in Complex Linear and Nonlinear Photonic Media*, Chaos Solitons Fractals **84**, 73 (2016).
[19] N. Akhmediev, J. M. Soto-Crespo, and A. Ankiewicz, *Extreme Waves That Appear from Nowhere: On the Nature of Rogue Waves*, Phys. Lett. A **373**, 2137 (2009).
[20] M. Mattheakis and G. P. Tsironis, in *Quodons in Mica: "Extreme Waves and Branching Flows in Optical Media"*, edited by J. F. R. Archilla, N. Jiménez, V. J. Sánchez-Morcillo, and L. M. García-Raffi (Springer International, Cham, 2015), pp. 425–454.
[21] A. Zannotti, *in Caustic Light in Nonlinear Photonic Media*, edited by A. Zannotti (Springer International, Cham, 2020), pp. 135–156.
[22] E. J. Heller, L. Kaplan, and A. Dahlen, *Refraction of a Gaussian Seaway*, J. Geophys. Res. Oceans **113** (2008).
[23] L. H. Ying, Z. Zhuang, E. J. Heller, and L. Kaplan, *Linear and Nonlinear Rogue Wave Statistics in the Presence of Random Currents*, Nonlinearity **24**, R67 (2011).
[24] H. Degueldre, J. J. Metzger, T. Geisel, and R. Fleischmann, *Random Focusing of Tsunami Waves*, Nat. Phys. **12**, 259 (2016).
[25] J. J. Metzger, R. Fleischmann, and T. Geisel, *Universal Statistics of Branched Flows*, Phys. Rev. Lett. **105**, 020601 (2010).
[26] J. J. Metzger, R. Fleischmann, and T. Geisel, *Statistics of Extreme Waves in Random Media*, Phys. Rev. Lett. **112**, 203903 (2014).
[27] M. Pradas, A. Pumir, and M. Wilkinson, *Uniformity Transition for Ray Intensities in Random Media*, J. Phys. A **51**, 155002 (2018).
[28] K. R. Fratus, R. A. Jalabert, and D. Weinmann, *Energy Stability of Branching in the Scanning Gate Response of Two-Dimensional Electron Gases with Smooth Disorder*, Phys. Rev. B **100**, 155435 (2019).
[29] H. Degueldre, J. J. Metzger, E. Schultheis, and R. Fleischmann, *Channeling of Branched Flow in Weakly Scattering Anisotropic Media*, Phys. Rev. Lett. **118**, 024301 (2017).
[30] A. Brandstötter, A. Girschik, P. Ambichl, and S. Rotter, *Shaping the Branched Flow of Light through Disordered Media*, Proc. Natl. Acad. Sci. U.S.A. **116**, 13260 (2019).
[31] L. Kaplan, *Statistics of Branched Flow in a Weak Correlated Random Potential*, Phys. Rev. Lett. **89**, 184103 (2002).
[32] J. J. Metzger, R. Fleischmann, and T. Geisel, *Intensity Fluctuations of Waves in Random Media: What Is the Semiclassical Limit?*, Phys. Rev. Lett. **111**, 013901 (2013).
[33] M. V. Berry, *Elementary Branching: Waves, Rays, Decoherence*, J. Opt. **22**, 115608 (2020).
[34] A. Startsev and Y. Stoilov, *On the Nature of Laser Polariton Tracks in Soap Films*, Quantum Electron. **34**, 569 (2004).
[35] J. Emile, O. Emile, and F. Casanova, *Light Guiding Properties of Soap Films*, Europhys. Lett. **101**, 34005 (2013).
[36] B. Crosignani, B. Daino, and P. Di Porto, *Light Scattering by a Rotating Disk*, J. Appl. Phys. **42**, 399 (1971).
[37] See Supplemental Material at http://link.aps.org/supplemental/10.1103/PhysRevX.12.021007 for derivation of the theory and further details on the experiments and simulation.
[38] L. Mandel and E. Wolf, *Optical Coherence and Quantum Optics* (Cambridge University Press, Cambridge, England, 1995).
[39] J. W. Goodman, *Statistical Optics* (Wiley, New York, 2015).
[40] M. V. Berry and C. Upstill, in *Progress in Optics*, edited by E. Wolf (Elsevier, New York, 1980), Vol. 18, pp. 257–346.